SCIENTIFIC REPORTS

OPEN

SUBJECT AREAS:
BIOPHYSICS
CELL BIOLOGY

Received
18 September 2013

Accepted
30 December 2013

Published
21 January 2014

Correspondence and requests for materials should be addressed to S.R. (sriram@tifrh.res.in) or G.V.S. (shiva.gvs@gmail.com)

* These authors contributed equally to this work.

Actomyosin contractility rotates the cell nucleus

Abhishek Kumar[1]*, Ananyo Maitra[2]*, Madhuresh Sumit[1], Sriram Ramaswamy[2,3] & G. V. Shivashankar[1]

[1]Mechanobiology Institute and Department of Biological Sciences, NUS, Singapore 117411, [2]Department of Physics, Indian Institute of Science, Bangalore 560012, India, [3]TIFR Centre for Interdisciplinary Sciences, Hyderabad 500075, India.

The cell nucleus functions amidst active cytoskeletal filaments, but its response to their contractile stresses is largely unexplored. We study the dynamics of the nuclei of single fibroblasts, with cell migration suppressed by plating onto micro-fabricated patterns. We find the nucleus undergoes noisy but coherent rotational motion. We account for this observation through a hydrodynamic approach, treating the nucleus as a highly viscous inclusion residing in a less viscous fluid of orientable filaments endowed with active stresses. Lowering actin contractility selectively by introducing blebbistatin at low concentrations drastically reduced the speed and coherence of the angular motion of the nucleus. Time-lapse imaging of actin revealed a correlated hydrodynamic flow around the nucleus, with profile and magnitude consistent with the results of our theoretical approach. Coherent intracellular flows and consequent nuclear rotation thus appear to be an intrinsic property of cells.

The nucleus of a eukaryotic cell is actively coupled to the dynamic cytoskeleton[1–4] by means of a variety of scaffold proteins: contractile actomyosin complexes[5,6], microtubule filaments constantly undergoing dynamic reorganization, and load bearing intermediate filaments[1–3,7–9]. It has long been known that the nucleus both translates and rotates in the cytoplasm in a variety of experimental situations[10–19]. While a number of molecular players including actin have been implicated in this context[1–4,9,12,15,20], we offer here a generic hydrodynamic understanding based on actomyosin contractility.

In this paper, we show that active stress is a critical component in determining nuclear movements. Fibroblast cells (NIH3T3) were plated on circular micro-patterned fibronectin surfaces to study the motion of the nucleus, independent of the effects of cell migration. Time-lapse imaging revealed a slow, systematic rotation of the nucleus, at a few degrees per minute, and a correlation between actin flow patterns and nuclear movement. We show that a hydrodynamic model of oriented filaments endowed with active contractile stresses[21–25], with the nucleus entering only as a passive inclusion, gives rise to the observed organized actin flow and nuclear rotation.

Two recent papers[26,27] on circulating flows of active fluids in confined geometries must be mentioned here. Fürthauer et al.[26] study the equations of hydrodynamics for active orientable fluids in a coaxial geometry with one cylindrical boundary fixed and one free to rotate. The interior of the inner cylinder did not enter their analysis. Woodhouse *et al.*[27], motivated by the phenomenon of cytoplasmic streaming[28,29], study suspensions of force dipoles in a circular geometry without a central inclusion; their predictions have been confirmed by Wioland *et al*[30]. The geometries studied in these related works differ in detail from ours, and their focus is not on the dynamics of the nucleus. Our studies suggest that nuclear rotation and circulating flows are an inherent property of the active cell interior under geometric confinement, a finding consistent with the above recent works, but in a context involving the dynamics of the nucleus.

Results

Geometric constraints on the cell affect the dynamics of the nucleus. To assess nuclear dynamics independent of cell migration, we used micro-patterned fibronectin-coated substrates to confine cells to circular regions. The spread area of the cells (1600 μm^2) was chosen to be close to the area that these cells occupy on unpatterned fibronectin coated dishes. Single cells were cultured on each patterned substrate and time-lapse phase-contrast imaging was carried out for about 8 hours. Fig. 1A shows the phase-contrast image and the color-coded intensity profile obtained by average intensity projection of the time-lapse images. This image clearly shows that the cellular shape is roughly circular and the concentration of actin is more-or-less homogeneous.

The translational and rotational movements of the nucleus were measured from the time-lapse images. Fig. 1B displays typical trajectories of one nucleolus, from which it is seen that the nucleus both rotates and translates, as

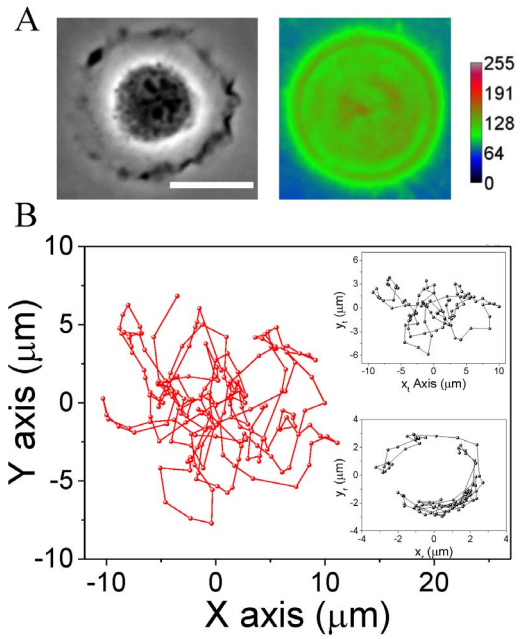

Figure 1 | Dynamics of the cell nucleus of a cell plated on a circular micropattern. (A) Phase-contrast image and corresponding color-coded average intensity projection for a cell plated on a circle of area 1600 μm^2. Scalebar = 20 μm. (B) Typical trajectory of one of the nucleoli. Inset: typical translational (top) and rotational (below) trace of nucleolar motion.

shown in Supplementary video 1. Since nuclear rotation in the vertical plane is negligible, we resolve the dynamics into two-dimensional translation and rotation in the horizontal or XY plane. Translation is estimated through the instantaneous mean position $(x_t,y_t)=\left(\frac{x_1+x_2}{2},\frac{y_1+y_2}{2}\right)$ of two nucleoli situated at roughly opposite points (x_1, y_1) and (x_2, y_2).

Nuclear rotation is characterized by determining the nuclear angle from the slope of the line formed between this mean position and one of the nucleoli and is given by $\theta=tan^{-1}\left(\frac{y_r}{x_r}\right)$ where $(x_r = x_1 - x_t)$ and $(y_r = y_1 - y_t)$. The instantaneous angular velocity is determined by $\frac{\delta\theta}{\delta t}=\frac{\theta'-\theta''}{\delta t}$ where θ' and θ'' are the nuclear rotational angle between consecutive time points with $\delta t = 5\ min$. A typical nuclear translation track for the nucleus is shown in the top inset to Fig. 1B while the bottom inset shows the rotational trajectory for the same nucleus.

Both translational and rotational movement of the nucleus during cell migration has been reported in the literature[10,11,15–18] for many cell types including NIH3T3 which was used in all our experiments. For completeness, we document nuclear dynamics during migration here as well. Supplementary Fig. S1A shows a representative DIC image of a monolayer of NIH3T3 cells cultured on a glass-bottomed dish. Time-lapse images (Supplementary Fig. S1B) of three cells from this field of view are presented with arrows showing the position of the nucleolus. Rotation and translation tracks of the nucleus are plotted for these cells in Supplementary Fig. S1C and D respectively, showing large departures from its initial position and orientation. We also see that the nuclear rotation can be large even when the translation is small, for cells located near the middle of the monolayer and therefore constrained at their periphery. Thus, we suspect that migration is not the unique underlying cause of the observed rotation. We therefore confine cells by plating them onto fibronectin patterns of well-defined geometries to see whether this alone can produce nuclear rotation. Though here we present results only for the circular geometry, we note that nuclear rotation is a robust feature which is also observed on other shapes like squares and triangles (Supplementary Fig. S2). On rectangles with high aspect ratio, the rotation is suppressed presumably because of the narrower confinement and elongation of the nucleus due to the elongated cell shape[31]. Noting that actomyosin contractility is a major supplier of internal force in the cell, it is natural to suspect that it has a crucial role to play in the phenomenon of nuclear rotation. To explore this connection, we turn now to the theory of active hydrodynamics[21–25] as applied to the cell interior.

Active fluid with a central inclusion. We show that cytoplasmic flows produced by actomyosin contractility are the minimal explanation for the observed rotation of the nucleus. To this end, we turn to the theoretical framework of active hydrodynamics[32–35]. Contractile stresses carried by actomyosin, given an arrangement of filaments compatible with the cell shape imposed by the pads and the presence of the nucleus as an internal obstacle, lead to organized flows that rotate the nucleus. More detailed propulsive elements, e.g., pushing by microtubules anchored onto the nuclear surface[7,36], while possibly present in the cell, are not a necessary part of the mechanism. It is also possible that nuclear rotation occurs for different reasons in different settings. Since the cell in the experiment is stretched, its height is smaller than its dimensions in the plane. We can therefore model it as a quasi-two-dimensional film with the hydrodynamics being cut off at a scale proportional to the height. We also assume an axisymmetric cell, and ignore treadmilling and the on-off kinetics of the motors. This highly simplified view of the cell still exhibits some key features of the dynamics found in the experiment.

Following a detailed calculation described below, we will see that contractility indeed leads to coherent circulating flows and hence to nuclear rotation. The physical mechanism underlying the flow in this geometry is closely related to the generic instability[32] of oriented active fluids. Filaments carrying stresses generated by actomyosin contractility generate no flow if they are uniformly aligned. A local perturbation in their orientation leads to inhomogeneities in local contractile stresses, to balance which viscous stresses, i.e., flow, is generated. The flow acts to tilt the filaments further in the direction in which they were perturbed, thus giving rise to an instability of the quiescent state. In a confined system this instability manifests itself only when, for a given scale of confinement, the actomyosin contractility crosses a threshold set by collective orientational relaxation. Beyond this critical value the active fluid can settle into a spontaneously moving steady state. In a planar geometry with one no-slip and one free-slip wall, the free boundary moves relative to the fixed one in this state[35]. Thus, it is intuitively clear that if an active fluid is present in an annular region, with the inner circle enclosing passive fluid and the outer boundary fixed, the passive fluid will be set in motion beyond some critical value of activity.

We now present the equations of active hydrodynamics[32–35]. The inner circular region represents the nucleus, which is taken to contain no active motor-filament complexes and is therefore modeled as a passive liquid drop of very high viscosity (η_n) - in effect undeformable. The outer annular region is the cytoplasm, which contains active orientable filaments. The inner fluid-fluid interface, i.e., the boundary between cytoplasm and nucleus, has tangential stress continuity and tangential velocity continuity, and the outer surface, the contact line of cell with pad, has no slip. We assume the filaments preferentially lie parallel to any surface with which they are in contact. In particular, they therefore lie tangent to both the inner and the outer boundaries.

The cytoplasmic medium is taken to consist of filaments suspended in the cytosol of viscosity $\eta_c \ll \eta_n$ (we will present results for $\eta_c/\eta_n = 1/5$). We assume the filaments are in a state of

well-formed local orientation whose magnitude does not change so that it can be characterized completely by a unit vector or "director" field, $\mathbf{n}(\mathbf{r})$[37], at position $\mathbf{r}$. Associated with the filaments is an active stress $\mathbf{W}\mathbf{n}(\mathbf{r})\mathbf{n}(\mathbf{r})$, where the parameter W is a measure of actomyosin activity. The concentration of filaments and myosin is assumed to be uniform. Fluid flow in the cytoplasm is described by the hydrodynamic velocity field $\mathbf{v}$. We define a molecular field conjugate to $\mathbf{n}$ as

$$\mathbf{h} = \boldsymbol{\delta}^{\mathrm{T}} \cdot \frac{\delta \mathrm{F}}{\delta \mathbf{n}} \tag{1}$$

where $\boldsymbol{\delta}^{\mathrm{T}} = \mathbf{I} - \mathbf{nn}$, with $\mathbf{I}$ being the unit tensor, projects onto a space transverse to $\mathbf{n}$. The equation of active hydrodynamics in steady state lead to a dynamic balance between shearing and relaxation of filaments[38],

$$\frac{\mathbf{h}}{\Gamma} = -\mathbf{v}\cdot\nabla\mathbf{n} + \Omega.\mathbf{n} + \lambda\boldsymbol{\delta}^{\mathrm{T}}\cdot(\mathbf{n}\cdot\mathbf{A}) \tag{2}$$

and force balance, ignoring inertia,

$$\nabla\cdot\boldsymbol{\sigma} = \zeta_c\mathbf{v} \tag{3}$$

with the total stress tensor

$$\boldsymbol{\sigma} = \eta_c\mathbf{A} - \mathrm{P}\mathbf{I} - \mathrm{W}\mathbf{nn} + \frac{1}{2}(\mathbf{nh} - \mathbf{hn}) - \frac{\lambda}{2}(\mathbf{nh} + \mathbf{hn}) - \boldsymbol{\sigma}^0 \tag{4}$$

Here, $\mathrm{F} = \int \mathrm{d}^{\mathrm{d}}\mathrm{x}\mathrm{f}, \mathrm{f} = (\mathrm{K}/2)(\nabla\mathbf{n})^2$ is the elastic free energy for the director $\mathbf{n}$, with the Frank elastic constant K, $\boldsymbol{\Omega}$ and $\mathbf{A}$ are respectively the symmetric and anti-symmetric components of the velocity gradient tensor, P is the pressure which serves here as a Lagrange multiplier to enforce overall incompressibility ($\nabla \cdot \mathbf{v} = 0$), and $\boldsymbol{\sigma}^0 = (\nabla\mathbf{n})\partial\mathrm{f}/\partial(\nabla\mathbf{n})$ is the Ericksen stress. We will work with a completely symmetric stress, $\boldsymbol{\sigma}$, built from $\boldsymbol{\sigma}$, which will give the same velocity field, due to angular momentum conservation[39,40].

The coefficient ζ_c in equation (3) represents in a z-averaged sense the effects of confinement on the damping of velocities. It has two contributions: a viscous part η_c/h^2 arising because flows within an adhered cell of thickness h in the vertical z-direction and no-slip at the base must in general have z-gradients on a scale h, and direct damping of flow through the kinetics of attachment and detachment of the cytoskeletal gel to the substrate. In our estimates below we retain only the viscous effect, so that ζ_c simply has the effect of screening the hydrodynamics at in-plane length-scales larger than h. Including attachment-detachment enhances ζ_c. We use circular polar coordinates (r, ϕ) in the plane. Since we assume axisymmetry, the radial velocity vanishes because incompressibility implies $\mathrm{d}v_r/\mathrm{dr} + v_r/\mathrm{r} = 0$, and $v_r = 0$ at both the interfaces. For force balance in the region corresponding to the nucleus we have to solve the equation

$$\frac{d^2v_\phi}{dr^2} + \frac{1}{r}\frac{dv_\phi}{dr} - \frac{v_\phi}{r^2} = \frac{2\zeta_n}{\eta_n}v_\phi \tag{5}$$

where $\zeta_n = \eta_n/h^2$. The equation can be solved in terms of Bessel functions, with the constraint that v_ϕ has to be 0 at $r = 0$. Continuity of tangential stress and velocity at the cytoplasm-nucleus interface gives the requisite number of boundary conditions.

Force balance in the azimuthal direction reads

$$\frac{d}{dr}\sigma^s_{\phi r} + \frac{2\sigma^s_{\phi r}}{r} = \zeta_c v_\phi \tag{6}$$

Expressing the director $\boldsymbol{n} = (n_\phi, n_r) = (cos\theta, sin\theta)$ the steady state equation (1) for the orientation field reads

$$\frac{1}{\Gamma}\frac{\delta F}{\delta\theta} = \frac{v_\phi}{r} + \lambda cos2\theta A_{r\phi} + \Omega_{r\phi} = (\lambda cos2\theta - 1)A_{r\phi} \tag{7}$$

Using equation (7), the $r\phi$ component of equation (4) can be recast as a first order differential equation for v_ϕ.

$$\frac{d}{dr}v_\phi = \frac{2Wsin2\theta + 4\sigma^S_{\phi r}}{2\eta_c + \Gamma(\lambda cos2\theta - 1)^2} + \frac{v_\phi}{r} \tag{8}$$

Thus, we have two first order equations, (8) and (6), and one second order equation (7) which we solve numerically to obtain an azimuthal velocity profile $v_\phi(r)$ as a function of radial position r.

A noticeable and robust feature of the solution (inset to Fig. 3A) is the presence of a maximum in the magnitude of the velocity some distance from the nucleus. This results from a combination of vanishing velocity at the outer boundary and the nuclear centre, and continuity of velocity and shear stress at the fluid-fluid interface. Note that our description does not include chiral effects, so that equivalent solutions with either sense of rotation are obtained.

The competition between active stresses that promote flow and orientational relaxation, that inhibits it, is contained in the dimensionless combination $= W/\zeta_c D = Wh^2/K$[35,41]. Accurate estimates of parameters for our system are not easy to make. The cytoskeletal active stress, W, is generally argued to be in the range 50–1000 Pa[42]. Frank constants for actin nematics appear to be 2–20 pN[43], as in ordinary thermotropic nematics. The thickness h of the spread cell in our experiments is about 1/5 of the lateral extent. For a spread cell area of 1600 μm^2 we therefore estimate $h = 8\ \mu m$. Taken together, this leads to $\alpha \sim 200$. However, if attachment-detachment contributions to ζ_c are included, α will be lowered substantially. From the active hydrodynamic model we know[32] that the system is quiescent for small values of this parameter. However, $\alpha = 4.9$, for which we present the results, is already sufficient to produce a spontaneous flow. Increasing α leads to increasingly complicated flows which we have only begun to explore. We do not attempt a detailed comparison between the observed and the theoretical flow patterns. However, the conclusion about the maximum of the velocity being away from the nucleus rests purely upon the confining geometry, and we expect that the time and angle averaged velocity profile, measured from the experiment, will have a peak away from the nuclear boundary.

For $\alpha \gg 1$ i.e an unbounded, oriented active fluid, one expects[32] spontaneous velocity gradients of order $\frac{W}{\eta_c}$. In[35] and[41] it was shown that the presence of confinement on a scale h modifies the above conclusion giving a characteristic rate $\frac{W}{\eta_c}F\left(\frac{h}{l}\right)$ where $F(x) \to 1$ as $x \to \infty$ and x^2 for $x \to 0$, where l is the in-plane scale associated with observation. In our case, $\frac{h}{l}$ is 1/5. Thus, the rotation rate should be of the order of $0.1W/\eta_c$. Using the arguments of[42] this estimate turns out to be of the order of a few degrees/min. This is reassuringly consistent with the magnitude obtained from the experiment.

The two predictions we can make based on this simple model are that actomyosin is crucial for nuclear rotation, and that the angle and time averaged angular velocity will be maximum away from the nucleus. We perform a series of experiments to check these. In the next sections, we study the contribution of actomyosin contractility to the translational and rotational dynamics of the nucleus.

Role of actomyosin contractility on nuclear dynamics. We test the role of contractility on nuclear dynamics to validate the theoretical predictions based on active fluids with an inclusion. Actomyosin contractility was altered by treating cells fully spread on the circular patterns with low concentration of blebbistatin, an inhibitor of the myosin II motor. We carried out live cell fluorescence confocal imaging to simultaneously visualize actin flow dynamics and nuclear rotation. Cells were transfected with lifeact-EGFP to label actin in live condition (Fig. 2). Time-lapse confocal imaging of actin revealed flow around the nucleus (Fig. 2A). To quantify the flow pattern (Supplementary Video 2), we carried out particle image velocimetry (PIV) analysis using MatPIV. This yielded flow vectors

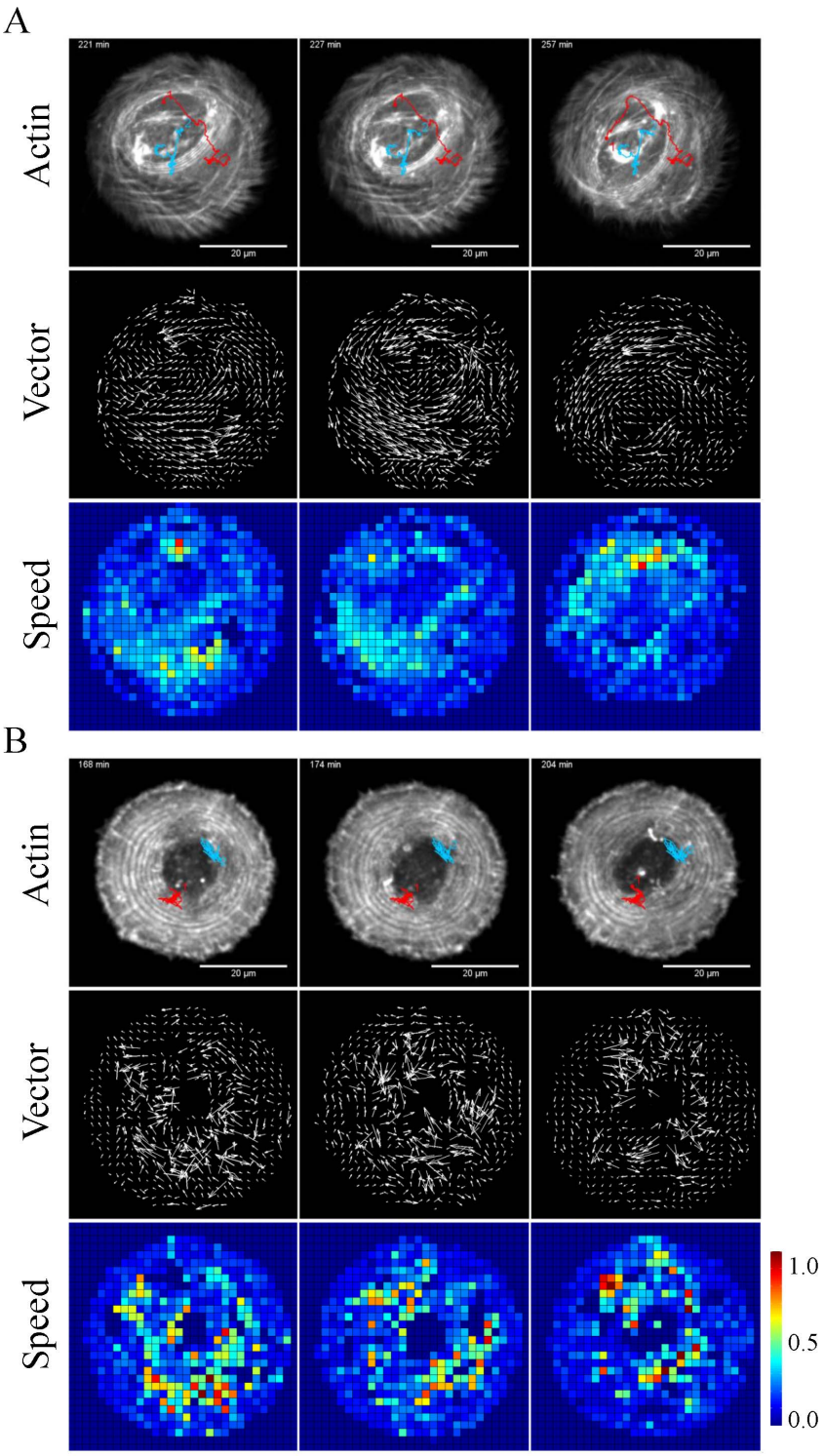

Figure 2 | Visualization of actin flow patterns during nuclear rotation in both control and blebbistatin treated cells plated on circular geometry. (A) Top panel: Tracks of two nucleoli (red and blue) showing both translational and rotational dynamics. Scale bar = 20 μm. Corresponding actin flow vectors (middle panel) and speed (last panel) was determined by particle image velocimetry (PIV) analysis using MatPIV for control (A) and blebbistatin (B) treated cells.

tangential to the nuclear boundary with direction correlated with that of the nuclear rotation as shown in Fig. 2A and Supplementary Video 3. Velocity field maps of actin flow were determined in small regions throughout the cell (Fig. 2A, last panel and Supplementary Video 4).

A circulating flow, required to rotate the nucleus, is clearly seen (Fig. 2A, middle panel and Supplementary Video 3 and 4). Interestingly, upon blebbistatin treatment, inward flow of actin (Supplementary Video 5–7), presumably driven by treadmilling, was not significantly affected. However, the azimuthal speed can be seen (Fig. 2B) to decrease substantially, despite some scatter in the data.

Further, we plot, in Fig. 3A and B, the angle averaged azimuthal velocity (v_ϕ), without and with blebbistatin respectively, inferred

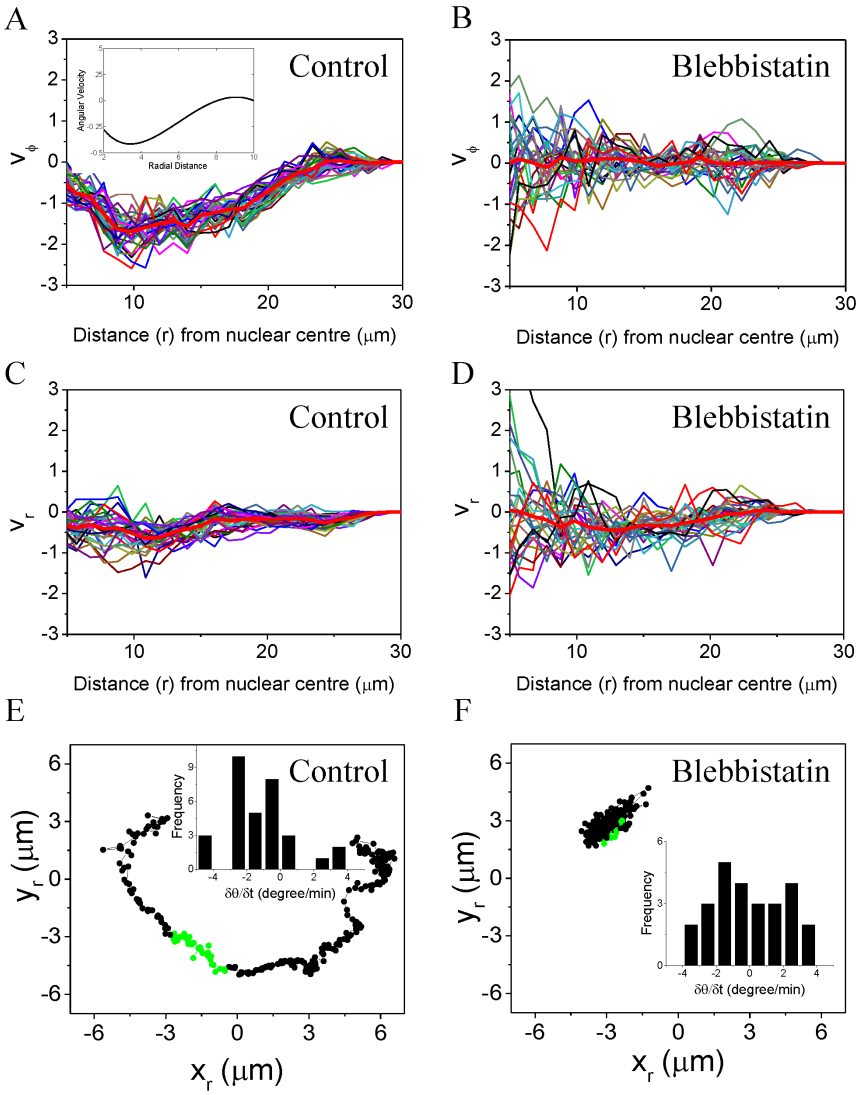

Figure 3 | Azimuthal and radial velocity of actin flow for cells plated on circular geometry. Plot of v_ϕ and v_r from velocity vectors of actin flow for control (A and C); and blebbistatin treated cells (B and D). Each color represents single time point from a single cell. The thick red curve is the mean of N such realizations (N = 30 for control and N = 25 for blebbistatin treated cell). Inset to 3A: a typical angular velocity vs. radial distance curve obtained by solving the equations (6)–(8) with parameter values mentioned in the text. Rotational traces of nuclear motion for control (E) and Blebbistatin treated (F) cells shown in Fig. 2. Azimuthal (3A and 3B) and radial (3C and 3D) actin flow velocities are plotted for control and Blebbistatin treated cell for the points marked in green in the trace. Inset to 3E and 3F: Histogram of instantaneous nuclear angular velocity for the two cases.

from PIV as a function of radial distance from the centre of the nucleus. For comparison we also show the radial velocity (v_r) (Fig. 3C and D). Note that the graphs start from the edge of the nucleus. As predicted from the theory (inset to Fig. 3A), the magnitude of the time-average (carried out over times corresponding to the green part of the nuclear trace shown in Fig. 3E) of azimuthal velocity peaks away from the nuclear boundary in the control cell. In blebbistatin treated cells, by contrast, the time-averaged velocity is close to 0, leading to the loss of nuclear rotation. However, (v_r) is small in both cases, albeit with slightly larger fluctuations in the presence of blebbistatin.

Concurrent with the vanishing of mean azimuthal actin flow upon blebbistatin treatment, the average angular velocity of the nucleus also significantly decreases to 0.07 with a spread of $\pm 0.83^\circ$/min when compared to $-1.17 \pm 0.33^\circ$/min for untreated cells (inset to Fig. 3E and 3F; time average performed over the part marked in green in the nuclear trace in Fig. 3E and F). We note that the average angular velocity of the nucleus is about twice the angle averaged actin velocity field at the edge of the nucleus. This possibly implies that the actin velocity is not equal to the hydrodynamic velocity. We further observe that fluctuations in both actin flow and nuclear angular velocity are enhanced for cells treated with blebbistatin. Although it is possible, within the hydrodynamic theory, to produce a state with irregular flow, termed "bacterial turbulence"[44] in another context, this requires entering the parameter regime where the steady spontaneous flow discussed here is unstable. It seems unlikely to us that the observed fluctuations are an instance of this phenomenon, as they are more pronounced in our experiments when blebbistatin suppresses myosin activity. We speculate that the origin of the fluctuations lies not in actomyosin contractility but in stochastic variation in biochemical activity or cytoskeletal remodeling. One would expect such fluctuations to be ironed out by the spontaneous flow, which is consistent with what we see in experiments.

Since there have been suggestions in the literature[15,36] that nuclear rotation is primarily driven by microtubules, we present results from studies of the response of nuclear movement to nocodazole, which interferes with microtubule polymerization. These experiments were conducted using triangular pads, in the course of studies of the effect

of varying the confining geometry. As seen in Supplementary Video 8, rotary motion of the nucleus still takes place, but is irregular, not consistent in direction, and accompanied by enhanced translational motion. This suggests that the nucleus is delocalized and not situated stably in the center of the cell, which is presumably why the rotation becomes incoherent. We also checked that suppressing dynein activity, by the addition of EHNA (Supplementary Video 9) and by over-expressing dynamitin (p50 sub-unit of dynactin, Supplementary Video 10), does not have a significant effect on the reported rotation. Thus, we can be reasonably confident that dynein-microtubule activity is not the major cause of nuclear rotation for cells on micropatterns. However, the detailed role of microtubules in nuclear rotation remains to be studied, and a theoretical study of a liquid-drop nucleus free to move around among active filaments remains to be done.

Further, we disrupted the actin filaments using latrunculin A. However, the cell did not adhere properly to the geometric pad due to the loss of actin filaments, and the motion of the nucleus became noisy and random (Supplementary Video 11). We conjecture that the rapidly changing boundary destabilizes the orientational order of the actin filaments in the interior, producing a noisy velocity field. Consequently, we did not observe a steadily rotating nucleus in our experiments. Gerashchenko *et al.*[45] have reported a higher instantaneous nuclear rotational velocity upon latrunculin B treatment. We think that one possible reason for this can be the lowering of cytosol viscosity due to the disintegration of the actin filaments.

Discussion

While several studies of nuclear rotation in migrating cells[15,20,45,46] imply that dynein and microtubules are responsible, our results on constrained single cells suggest an important role for actomyosin contractility, at least in non-migrating cells. We offer a simple theoretical explanation for the rotation in which the nucleus is modeled as a nearly rigid inclusion in the cytoplasm treated as a fluid containing filaments endowed with intrinsic stresses. The result is an angular velocity profile with a maximum magnitude at a radial position intermediate between the nucleus and the cell periphery, as observed in the experiments, and nonzero at the nuclear surface, corresponding to nuclear rotation. The predicted magnitude of the rotation rate based on plausible estimates of material parameters is also consistent with the measurements. That blebbistatin treatment greatly suppresses the flow lends support to our proposed generic mechanism. This does not imply that the nucleus of every cell-type will rotate in all situations. At least two mechanisms could contribute to suppressing the generic instability that leads to circulating flows. One, in the absence of a reasonably rigid geometry, the cell boundary is free to change shape. This would disrupt the imposed boundary orientation of the filaments, and hence the orderly pattern of active particles needed to drive a coherent flow. Two, the apical actin fibers[47–51], absent in square and circular geometries, present to some extent in triangular geometries, and very well formed in elongated geometries, bear down on and thus enhance the friction on the nucleus, suppressing its motion.

Collectively, our results highlight the importance of actomyosin contractility for nuclear dynamics. We hope our work leads to wider studies of the manifestations of nuclear rotation, its possible biological consequences, and an understanding of how cells suppress such effects.

Methods

Cell culture and drug treatment. NIH3T3 fibroblasts (ATCC) were cultured in low glucose DMEM (Invitrogen) supplemented with 10% Fetal Bovine Serum (FBS) (Gibco, Invitrogen) and 1% Penicillin-Streptomycin (Invitrogen). Cells were maintained at 37°C in incubator with 5% CO_2 in a humidified condition. Cells were trypsinized and seeded on fibronectin coated patterned surfaces for 3 hours before staining or imaging. For confocal imaging, untreated hydrophobic dishes (Ibidi) with micropatterns were used. 65,000 cells were seeded on the micropatterned surfaces (with 10,000 patterns) for 30 minutes, after which the non-adhered cells were removed and fresh media was re-added in the dishes. All the control experiments were carried out without any treatment. Blebbistatin (Sigma) was serially diluted from high concentration (68 mM) stock using filtered media to the final concentration (1.25 μM).This minimizes the effect of any other solvent like DMSO. Nocodazole (Sigma), Latrunculin A (Sigma) and EHNA (sigma) were used at 0.25 μg/ml, 100 nM and 20 μg/ml respectively. All drugs were added after cells had fully adhered to the micropatterns and imaging was carried out atleast 1hour after the addition of the drugs.

Preparation of PDMS stamps and micro-contact printing. PDMS stamps were prepared from the PDMS Elastomer (SYLGARD 184, DOW Corning) and the ratio of curing agent to the precursor used was 1 : 10. The curing agent and the precursor were mixed homogeneously before pouring onto the micropatterned silicon wafer. The mixture was then degassed in the desiccator for at least 30 minutes to remove trapped air bubbles and cured at 80°C for 2 hours. Then, the stamps were peeled off from the silicon wafer. Micropatterned PDMS stamps were oxidized and sterilized under high power in Plasma Cleaner (Model PDC-002, Harrick Scientific Corp) for 4 minutes. 30 μl of 100 μg/ml fibronectin solution (prepared by mixing 27 μl of 1 × PBS to 1.5 μg of 1 mg/ml fibronectin and 1.5 μl of Alexa 647 conjugated fibronectin) was allowed to adsorb onto the surface of each PDMS stamp under sterile condition for 20 minutes before they were dried using a tissue paper. The PDMS stamp was then deposited onto the surface of an untreated hydrophobic dish (Ibidi) (for High-resolution imaging) to transfer the micro-features. Each patterned dish was inspected using a fluorescent microscope to verify the smooth transfer of fibronectin micropatterns and was treated with 1 ml of 2 mg/ml Pluronic F-127 for 2 hours to passivate its non-fibronectin coated regions.

Cell transfection. Transfection of Lifeact EGFP (for imaging actin dynamics) and dynamitin (p50 subunit of dynactin complex) (a gift from Alexander Bershadsky's lab, MBI, Singapore) in wt NIH3T3 cells was carried out using JetPRIMEpolyplus transfection kit. 1 μg of plasmid was mixed in 100 μl of JetPRIME buffer by vortexing and spinning, 3.5 μl of JetPRIME reagent was then added and the mixture was again vortexed and spun. The mixture was incubated for 30 minutes and then added to a 50–60% confluent culture in 35 mm dish. The cells were kept in the fresh media for 2 hours before adding the transfection mixture. Cells were incubated for 20 hours before plating them on the patterned substrate.

Imaging. Phase-contrast imaging of cells on different geometrical patterns was performed using Nikon Biostation IMq using 40× objective at 37°C in a humidified chamber with 5% CO_2. Confocal time-lapse imaging of the cells transfected with Lifeact EGFP was carried out using Nikon A1R with 60×, 1.4 NA oil objective at 37°C in a humidified incubator with 5% CO_2.

Image analysis and quantifications. Acquired images were processed and analysed using ImageJ software (http://rsbweb.nih.gov/ij/index.html). To determine the translational coordinates and the rotational angle of the nucleus, diagonally opposite nucleoli were manually tracked from the phase-contrast image of the cell using the ImageJ plugin- MtrackJ (http://www.imagescience.org/meijering/software/mtrackj/). The nucleoli can be clearly seen in these images without any further fluorescence labelling (Fig. 1). The nucleoli were used to track the nuclear dynamics as their positions are stable during interphase of cell cycle[12,46]. All our analysis is confined to this time period during cell cycle. Nuclear translation is estimated through the instantaneous mean position of two nucleoli situated at roughly diametrically opposed points. Nuclear angle was determined from the slope of the line formed between the centroid and a nucleolus.

Particle image velocimetry (PIV) analysis was carried out using Matlab PIV toolbox-Matpiv between consecutive image frames separated by 1 min. Images acquired were 512 × 512 pixels. Size of interrogation window was chosen to be 32 × 32 with an overlap of 50% between the consecutive time frames. "Single pass" method was used for calculating the velocities. The speed and angle of actin flow vectors (Fig. 3) was determined from the correlation of these interrogation windows with their neighbouring ones. Azimuthal (v_ϕ) and radial (v_r) velocities were calculated from the actin flow speed. Velocity components in radial and angular coordinate are as follows: $v_r = \frac{1}{r}\left(x \cdot v_x + y \cdot v_y\right)$ and $v_\phi = \frac{1}{r}\left(x \cdot v_y - y \cdot v_x\right)$, where, $r = \sqrt{x^2 + y^2}$ is the radial distance from the centre of nucleus and v_x and v_y are the actin flow velocity components determined from PIV analysis along x and y direction/axis measured from centre of nucleus. Quantifications were done using programs written in either LabVIEW 6.1 or MATLAB R2010a. All the graphs and curve fittings, except for inset to Fig. 3C were carried out using OriginPro 8.1 (OriginLab Corporation, Northampton, USA). Fig. 3C was generated by numerically solving (equations 6–8) in MATLAB R2010a.

1. Crisp, M. *et al.* Coupling of the nucleus and cytoplasm: role of the LINC complex. *J. Cell Biol.* **172**, 41–53 (2006).
2. Haque, F. *et al.* SUN1 interacts with nuclear lamin A and cytoplasmic nesprins to provide a physical connection between the nuclear lamina and the cytoskeleton. *Mol Cell Biol* **26**, 3738–3751 (2006).
3. Houben, F., Ramaekers, F. C., Snoeckx, L. H. & Broers, J. L. Role of nuclear lamina-cytoskeleton interactions in the maintenance of cellular strength. *Biochim Biophys Acta* **1773**, 675–686 (2007).

4. Wang, N., Tytell, J. D. & Ingber, D. E. Mechanotransduction at a distance: mechanically coupling the extracellular matrix with the nucleus. *Nat Rev Mol Cell Biol* **10**, 75–82 (2009).
5. Takiguchi, K. Heavy meromyosin induces sliding movements between antiparallel actin filaments. *J Biochem* **109**, 520–527 (1991).
6. Bendix, P. M. *et al.* A quantitative analysis of contractility in active cytoskeletal protein networks. *Biophys J* **94**, 3126–3136 (2008).
7. King, M. C., Drivas, T. G. & Blobel, G. A network of nuclear envelope membrane proteins linking centromeres to microtubules. *Cell* **134**, 427–438 (2008).
8. Thery, M., Pepin, A., Dressaire, E., Chen, Y. & Bornens, M. Cell distribution of stress fibres in response to the geometry of the adhesive environment. *Cell Motil Cytoskelet.* **63**, 341–355 (2006).
9. Tzur, Y. B., Wilson, K. L. & Gruenbaum, Y. SUN-domain proteins: "Velcro" that links the nucleoskeleton to the cytoskeleton. *Nat Rev Mol Cell Biol* **7**, 782–788 (2006).
10. Houben, F. *et al.* Disturbed nuclear orientation and cellular migration in A-type lamin deficient cells. *Biochim Biophys Acta* **1793**, 312–324 (2009).
11. Maninova, M. *et al.* The reorientation of cell nucleus promotes the establishment of front-rear polarity in migrating fibroblasts. *J Mol Biol* **425**, 2039–2055 (2013).
12. Brosig, M., Ferralli, J., Gelman, L., Chiquet, M. & Chiquet-Ehrismann, R. Interfering with the connection between the nucleus and the cytoskeleton affects nuclear rotation, mechanotransduction and myogenesis. *Int J Biochem Cell Biol* **42**, 1717–1728 (2010).
13. Hagan, I. & Yanagida, M. Evidence for cell cycle-specific, spindle pole body-mediated, nuclear positioning in the fission yeast Schizosaccharomyces pombe. *J Cell Sci* **110 (Pt 16)**, 1851–1866 (1997).
14. Lee, J. S., Chang, M. I., Tseng, Y. & Wirtz, D. Cdc42 mediates nucleus movement and MTOC polarization in Swiss 3T3 fibroblasts under mechanical shear stress. *Mol Biol Cell* **16**, 871–880 (2005).
15. Levy, J. R. & Holzbaur, E. L. Dynein drives nuclear rotation during forward progression of motile fibroblasts. *J Cell Sci* **121**, 3187–3195 (2008).
16. Luxton, G. W., Gomes, E. R., Folker, E. S., Vintinner, E. & Gundersen, G. G. Linear arrays of nuclear envelope proteins harness retrograde actin flow for nuclear movement. *Science* **329**, 956–959 (2010).
17. Reinsch, S. & Gonczy, P. Mechanisms of nuclear positioning. *J Cell Sci* **111 (Pt 16)**, 2283–2295 (1998).
18. Starr, D. A. Communication between the cytoskeleton and the nuclear envelope to position the nucleus. *Mol Biosyst* **3**, 583–589 (2007).
19. Bard, F., Bourgeois, C. A., Costagliola, D. & Bouteille, M. Rotation of the cell nucleus in living cells: a quantitative analysis. *Biol Cell* **54**, 135–142 (1985).
20. Vicente-Manzanares, M., Zareno, J., Whitmore, L., Choi, C. K. & Horwitz, A. F. Regulation of protrusion, adhesion dynamics, and polarity by myosins IIA and IIB in migrating cells. *J Cell Biol* **176**, 573–580 (2007).
21. Joanny, J. F., Julicher, F., Kruse, K. & Prost, J. Hydrodynamic theory for multi-component active polar gels. *New J. Phys.* **9**, (2007).
22. Julicher, F., Kruse, K., Prost, J. & Joanny, J. F. Active behavior of the cytoskeleton. *Phys. Reports-Review Sect. Phys. Lett.* **449**, 3–28 (2007).
23. Ramaswamy, S. The Mechanics and Statistics of Active Matter. *Annu. Rev. Condens. Matter Physics, Vol 1* **1**, 323–345 (2010).
24. Toner, J., Tu, Y. H. & Ramaswamy, S. Hydrodynamics and phases of flocks. *Ann. Phys. (N. Y).* **318**, 170–244 (2005).
25. Marchetti, M. C. *et al.* Hydrodynamics of soft active matter. *Rev. Mod. Phys.* **85**, (2013).
26. Furthauer, S., Neef, M., Grill, S. W., Kruse, K. & Julicher, F. The Taylor-Couette motor: spontaneous flows of active polar fluids between two coaxial cylinders. *New J. Phys.* **14**, (2012).
27. Woodhouse, F. G. & Goldstein, R. E. Spontaneous circulation of confined active suspensions. *Phys Rev Lett* **109**, 168105 (2012).
28. Goldstein, R. E., Tuval, I. & van de Meent, J. W. Microfluidics of cytoplasmic streaming and its implications for intracellular transport. *Proc Natl Acad Sci U S A* **105**, 3663–3667 (2008).
29. Verchot-Lubicz, J. & Goldstein, R. E. Cytoplasmic streaming enables the distribution of molecules and vesicles in large plant cells. *Protoplasma* **240**, 99–107 (2010).
30. Wioland, H., Woodhouse, F. G., Dunkel, J., Kessler, J. O. & Goldstein, R. E. Confinement Stabilizes a Bacterial Suspension into a Spiral Vortex. *Phys. Rev. Lett.* **110**, (2013).
31. Khatau, S. B. *et al.* A perinuclear actin cap regulates nuclear shape. *Proc Natl Acad Sci U S A* **106**, 19017–19022 (2009).
32. Aditi Simha, R. & Ramaswamy, S. Hydrodynamic fluctuations and instabilities in ordered suspensions of self-propelled particles. *Phys Rev Lett* **89**, 58101 (2002).
33. Kruse, K., Joanny, J. F., Julicher, F., Prost, J. & Sekimoto, K. Asters, vortices, and rotating spirals in active gels of polar filaments. *Phys Rev Lett* **92**, 78101 (2004).
34. Liverpool, T. B. & Marchetti, M. C. Instabilities of isotropic solutions of active polar filaments. *Phys Rev Lett* **90**, 138102 (2003).
35. Voituriez, R., Joanny, J. F. & Prost, J. Spontaneous flow transition in active polar gels. *Europhys. Lett.* **70**, 404–410 (2005).
36. Wu, J., Lee, K. C., Dickinson, R. B. & Lele, T. P. How dynein and microtubules rotate the nucleus. *J Cell Physiol* **226**, 2666–2674 (2011).
37. Gennes, P. G. de & Prost, J. *The physics of liquid crystals. Oxford Sci. Publ.* xvi, 597 p. (Clarendon Press; Oxford University Press, 1993).
38. Stark, H. & Lubensky, T. C. Poisson-bracket approach to the dynamics of nematic liquid crystals. *Phys Rev E Stat Nonlin Soft Matter Phys* **67**, 61709 (2003).
39. Landau, L. D., Lifshitz, E. M., Kosevich, A. d. M. & Pitaevskii, L. P. *Theory of elasticity. Course Theor. Phys.* viii, 187 p. (Pergamon Press, 1986).
40. Martin, P., Parodi, O. & Pershan, P. Unified Hydrodynamic Theory for Crystals, Liquid Crystals, and Normal Fluids. *Phys. Rev. A* **6**, 2401–2420 (1972).
41. Ramaswamy, S. & Rao, M. Active-filament hydrodynamics: instabilities, boundary conditions and rheology. *New J. Phys.* **9**, (2007).
42. Joanny, J. F. & Prost, J. Active gels as a description of the actin-myosin cytoskeleton. *HFSP J.* **3**, 94–104 (2009).
43. Lai, G. H. *et al.* Self-Organized Gels in DNA/F-Actin Mixtures without Crosslinkers: Networks of Induced Nematic Domains with Tunable Density. *Phys. Rev. Lett.* **101**, (2008).
44. Dunkel, J. *et al.* Fluid dynamics of bacterial turbulence. *Phys Rev Lett* **110**, 228102 (2013).
45. Gerashchenko, M. V., Chernoivanenko, I. S., Moldaver, M. V. & Minin, A. A. Dynein is a motor for nuclear rotation while vimentin IFs is a "brake" *Cell Biol Int* **33**, 1057–1064 (2009).
46. Ji, J. Y. *et al.* Cell nuclei spin in the absence of lamin b1. *J Biol Chem* **282**, 20015–20026 (2007).
47. Mazumder, A. & Shivashankar, G. V. Gold-nanoparticle-assisted laser perturbation of chromatin assembly reveals unusual aspects of nuclear architecture within living cells. *Biophys J* **93**, 2209–2216 (2007).
48. Mazumder, A. & Shivashankar, G. V. Emergence of a prestressed eukaryotic nucleus during cellular differentiation and development. *J R Soc Interface* **7 Suppl 3**, S321–30 (2010).
49. Khatau, S. B., Kim, D. H., Hale, C. M., Bloom, R. J. & Wirtz, D. The perinuclear actin cap in health and disease. *Nucleus* **1**, 337–342 (2010).
50. Versaevel, M., Grevesse, T. & Gabriele, S. Spatial coordination between cell and nuclear shape within micropatterned endothelial cells. *Nat Commun* **3**, 671 (2012).
51. Li, Q., Kumar, A., Makhija, E. & Shivashankar, G. V. The regulation of dynamic mechanical coupling between actin cytoskeleton and nucleus by matrix geometry. *Biomaterials* **35**, 961–969 (2014).

Acknowledgments

A.K., M.S. and G.V.S. thank the Mechanobiology Institute (MBI) at the National University of Singapore (NUS) for funding and MBI facility. A.M. thanks TCIS, TIFR Hyderabad for support and hospitality, and S.R. acknowledges a J.C. Bose fellowship.

Author contributions

A.K. and G.V.S. designed the experiment. A.K. and M.S. performed the experiment. A.K., M.S. and G.V.S. analysed the data. A.M. and S.R. formulated and simulated the theoretical model. A.K., A.M., S.R. and G.V.S. wrote the paper.

Additional information

Supplementary information accompanies this paper at http://www.nature.com/scientificreports

Competing financial interests: The authors declare no competing financial interests.

How to cite this article: Kumar, A., Maitra, A., Sumit, M., Ramaswamy, S. & Shivashankar, G.V. Actomyosin contractility rotates the cell nucleus. *Sci. Rep.* **4**, 3781; DOI:10.1038/srep03781 (2014).